Journal of Computational Physics 227 (2008) 9554–9571

Contents lists available at ScienceDirect

Journal of Computational Physics

journal homepage: www.elsevier.com/locate/jcp

Modeling the magnetic interactions between paramagnetic beads in magnetorheological fluids

Eric E. Keaveny, Martin R. Maxey *

Division of Applied Mathematics, Brown University, 182 George Street, Box F, Providence, RI 02912, USA

ARTICLE INFO

Article history:
Received 14 March 2008
Received in revised form 18 June 2008
Accepted 3 July 2008
Available online 22 July 2008

Keywords:
Magnetorheological fluids
Magnetic dipoles
Multipole methods
Superparamagnetic particles
Particle self-assembly

ABSTRACT

In this study, we develop and compare new and existing methods for computing the magnetic interactions between paramagnetic particles in magnetorheological (MR) fluids. The commonly employed point-dipole methods are outlined and the inter-particle magnetic forces, given by these representations, are compared with exact values. An alternative finite-dipole model, where the magnetization of a particle is represented as a distribution of current density, is described and the associated computational effort is shown to scale as $O(N)$. As the dipole moments and forces given by this model depend on the length scale of the current distribution, a sensitivity analysis is performed to reveal a proper choice of this length scale. While the dipole models give a good estimation of the far-field interactions, as two particles come into contact, higher order multipoles are needed to properly resolve their interaction. We present the exact two-body calculation and describe a procedure to include the higher multipoles arising in a pairwise interaction into a dipole model. This inclusion procedure can be integrated with any dipole or higher-multipole calculation. Results from relevant three-body problems are compared to exact solutions to provide information as to how well the inclusion procedure performs in simulations of self-assembly and estimating the yield strength of structures.

1. Introduction

Superparamagnetic particles, ranging from 0.3 to 10 μm in diameter, suspended in a liquid will aggregate to form chains when an initially random dispersion is placed in a uniform, static magnetic field. The formation of these fibrous structures changes the bulk rheological properties of the medium and as such these suspensions are typically referred to as magnetorheological fluids (MR) [1]. Traditionally, MR fluids have been employed in a variety of damping and shock absorbing devices where the particle volume fractions for the suspensions range from 20% to 40%. In this context, the particles are usually carbonyl iron powders suspended in oil and are subject to strong magnetic fields, in excess of 10^5 A/m. Such MR fluids differ from ferrofluids [2] that consist of colloidal suspensions of nanoscale ferromagnetic particles, typically single domain magnetite crystals 10 nm in diameter. In ferrofluids, the particles have a surfactant coating that prevents permanent aggregation and Brownian motion is very significant, inhibiting the formation of particle structures. More recently, superparamagnetic particles and the structures that they form have been employed in a variety of micro-fluidic devices. These monodisperse polymeric spherical particles containing randomly oriented magnetite crystals are key components in recently developed DNA separation chips [3] and micro-mixers [4]. Small groups of particles can be manipulated to form micro-pumps in a channel [5], or joined together to a produce magnetic filament [6,7] that provides the propulsive mechanism for an artificial micro-swimmer [8,9].

* Corresponding author. Tel.: +1 401 863 1482; fax: +1 401 863 2722.
E-mail addresses: maxey@dam.brown.edu, maxey@cfm.brown.edu (M.R. Maxey).

0021-9991/$ - see front matter © 2008 Elsevier Inc. All rights reserved.
doi:10.1016/j.jcp.2008.07.008

Regardless of the application, a simulation of micron-sized paramagnetic particles requires the computation of the hydrodynamic, magnetic, Brownian, and possible surface forces between the beads. When considering suspensions of many beads, these forces need to be addressed through thoughtful modeling to provide an accurate description of the physics using computationally efficient algorithms. In this study, we concern ourselves with models of the magnetic interactions between paramagnetic particles that have a low magnetic susceptibility and exhibit minimal hysteresis. We further limit our discussion to cases where the magnetization of a particle responds linearly to the applied field. This assumption suffices for the magnitudes of magnetic field employed in micro-fluidic applications mentioned above, for lab-on-a-chip devices [10] or structured materials [11], and over a certain range for standard MR fluids [12].

For a linearly susceptible material, an exact computation of the magnetic interactions involves generating the solution to Laplace's equation subject to the appropriate boundary conditions [13,14]. The force on a given bead is then determined by formulating the Maxwell stress tensor from the resultant field and integrating the normal projection of this tensor over the bead's surface. This process is rather cumbersome and is only viable when considering systems of very few particles in symmetric configurations [15]. As a result, only dipole–dipole interactions are usually considered in simulations and in theoretical studies of MR fluids [16–19]. Such point-dipole methods require two steps. First, the values of the induced dipole moments for each particle need to be determined. Depending on the number of particles, this calculation can require solving a large system of linear equations. Once the dipole moments are computed, the resulting interparticle magnetic forces can be evaluated. This calculation requires depleted sums to avoid self-singular terms and scales inherently as $O(N^2)$ where N is the number of particles.

Although dipole simulations illustrate the general behavior of the aggregates, a more detailed description of the magnetic interactions is necessary to accurately quantify chain deformation and yield strengths in micro-fluidic devices. Beyond the point-dipoles description mentioned above, Ly et al. [20] have employed a combination of fast multipole methods (FMM) and boundary integral computations to resolve the magnetic interactions in two-dimensional systems. Far-field interactions can be handled efficiently by FMM [21], where the domain is divided into cells and the effects of source terms in a distant cell are represented by a summed multipole series based on the moments of these source terms. Other models have been developed to simulate the interactions between dielectric particles in electrorheological (ER) fluids. Klingenberg et al. [22,23] determined the field resulting from two dielectric spheres in a uniform field from which they constructed an interparticle force function. With this functional form of the force, a molecular dynamics type of simulation was performed. Bonnecaze and Brady [24–26] approached the problem by constructing an approximate grand capacitance matrix. The matrix relates the multipole moments of each particle to the electric potential and its derivatives evaluated at the particles' locations, and aims to capture both the many-body, dipole interactions and the local two-body, higher multipole interactions. From this matrix, the electrostatic energy density is determined and differentiated to obtain the interparticle forces.

The purpose of this study is twofold. First, we develop a new model to accelerate the calculation of many-body dipole interactions. In this model, each bead's magnetization is represented as a finite distribution of current density. This eliminates the need for depleted sums to avoid singular self-interaction terms. For a sufficiently large number of particles the computational complexity scales as $O(N)$ where N is the number of particles. The finite nature of the distributions allows the model to be implemented with a variety of numerical algorithms or in combination with FMM solvers. Second, we present the exact solution to the two-body problem and introduce a technique to blend this result with a many-body dipole calculation. This inclusion procedure is general and can be used in conjunction with the finite dipole method presented here or any other dipole or higher-order multipole method.

To begin, we state the general magnetostatic problem that all the models address. We summarize and describe the point-dipole models commonly used in MR fluid simulations. The interparticle forces given by these dipole methods are compared to exact calculations. We then formulate and present the finite-dipole model through exact solutions to Maxwell's equations and establish an iterative method to solve for particle interactions. The exact two-body calculation is described and from this calculation the far-field modification procedure is explained and implemented in a series of three-body problems.

2. Magnetostatic problem

Consider N spheres of radius a and permeability μ located $\mathbf{Y}^{(n)},\ n = 1,\ldots,N$, and subject to a uniform magnetic field $\mathbf{H}_0$. Since the fluid phase is assumed to have zero susceptibility, the permeability of fluid is that of free space, μ_0. Further, if there are no free currents in the system, Maxwell's equations [13,14] are

$$\nabla \cdot \mathbf{B} = 0, \tag{1}$$

$$\nabla \times \mathbf{H} = \mathbf{0} \tag{2}$$

with the magnetic flux density $\mathbf{B} = \mu_0 \mathbf{H}$ in the fluid and $\mathbf{B} = \mu \mathbf{H}$ in each sphere. Eq. (2) allows the introduction of the scalar potentials such that $\mathbf{H} = -\nabla \Phi_{\text{out}}$ in the fluid phase and $\mathbf{H} = -\nabla \Phi_{\text{in}}^{(n)}$ inside sphere n for $n = 1,\ldots,N$. From the relationships between $\mathbf{B}$ and $\mathbf{H}$ and (1), we arrive at Laplace's equation for the fluid and particle phases,

$$\nabla^2 \Phi_{\text{out}} = 0, \tag{3}$$

$$\nabla^2 \Phi_{\text{in}}^{(n)} = 0. \tag{4}$$

For a coordinate system whose origin is located at $\mathbf{Y}^{(n)}$, we define $\mathbf{r}_n = \mathbf{x} - \mathbf{Y}^{(n)}$ with $r_n = |\mathbf{r}_n|$ and $\hat{\mathbf{r}}_n = \mathbf{r}_n/r_n$. At the surface of each sphere, the conditions

$$\hat{\mathbf{r}}_n \cdot (\mathbf{B}_{\text{out}} - \mathbf{B}_{\text{in}}) = 0, \tag{5}$$

$$\hat{\mathbf{r}}_n \times (\mathbf{H}_{\text{out}} - \mathbf{H}_{\text{in}}) = 0 \tag{6}$$

require the potential satisfy

$$\Phi_{\text{in}}^{(n)} = \Phi_{\text{out}}, \tag{7}$$

$$\mu \frac{\partial \Phi_{\text{in}}^{(n)}}{\partial r_n} = \mu_0 \frac{\partial \Phi_{\text{out}}}{\partial r_n} \tag{8}$$

at $r_n = a$ for $n = 1, \ldots, N$. Additionally, as $r_n \to \infty$

$$\Phi_{\text{out}} \to -\mathbf{H}_0 \cdot \mathbf{r}_n. \tag{9}$$

After solving for the potential and computing the field, the Maxwell stress tensor, given in index notation by

$$T_{ij} = \mu_0 H_i H_j - \frac{\mu_0}{2} \delta_{ij} H_k H_k \tag{10}$$

is formed from the exterior field with $\mathbf{H} = \mathbf{H}_{\text{out}}$ and the resultant force on bead n is determined from the surface integral

$$\mathbf{F}_n = a^2 \int_0^{2\pi} \int_0^{\pi} \mathbf{T} \cdot \hat{\mathbf{r}}_n \sin\theta_n \, \mathrm{d}\theta_n \, \mathrm{d}\phi_n, \tag{11}$$

where θ_n and ϕ_n denote the zenith and azimuth angles respectively for the spherical coordinate system whose origin is located at $\mathbf{Y}^{(n)}$. The general solution to (3) can, in principle, be written down as a sum of the potential due to the external magnetic field and the sum of N spherical harmonic expansions, where the expansion for the nth particle has the origin located at $\mathbf{Y}^{(n)}$. The complications arise through application of the boundary conditions (7) and (8) when one must truncate the expansions retaining L multipoles and relate the different coordinate systems to each other. Even if this is done successfully, one is left with, in general, an unwieldy linear system of equations to determine the unknown coefficients in each expansion. All the models presented are, in some way, a reduction of this general problem. Each model is classified not only by the degree to which the particles interact (dipole, quadrupole, etc.) but also by how many particles are involved in each interaction (two-body, three-body, etc.).

2.1. Fixed dipole model

The simplest and most commonly used model is the fixed dipole model. In this model, only the magnetization induced by the external field is considered. Thus, the basis of this model is the solution to the general problem described for a single, isolated particle ($N = 1$). The coordinate system is aligned so $\mathbf{H}_0 = H_0\hat{\mathbf{z}}$. Symmetry conditions impose the lack of azimuthal dependence of the solution and the boundary conditions eliminate terms other than the $P_1(\cos\theta)$ term in the spherical harmonic expansion. The solution is, see [14],

$$\Phi_{\text{in}} = -H_0 \frac{3\mu_0}{\mu + 2\mu_0} r\cos\theta, \tag{12}$$

$$\Phi_{\text{out}} = -H_0 r\cos\theta + H_0 a^3 \frac{\mu - \mu_0}{\mu + 2\mu_0} \frac{\cos\theta}{r^2}. \tag{13}$$

For a linearly susceptible material, the induced magnetic dipole density $\mathbf{M} = \chi\mathbf{H}_{\text{in}}$, with $\chi = \mu/\mu_0 - 1$. The dipole moment, $\mathbf{m}$, is therefore

$$\mathbf{m} = \int_{\text{sphere}} \mathbf{M} \, \mathrm{d}^3\mathbf{x} = \int_{\text{sphere}} \chi\mathbf{H}_{\text{in}} \, \mathrm{d}^3\mathbf{x} = \frac{4}{3}\pi a^3 \chi_{\text{eff}} \mathbf{H}_0, \tag{14}$$

where $\chi_{\text{eff}} = 3\chi/(\chi + 3)$. The field resulting from second term in (13) is equal to that due to a point dipole of strength $\mathbf{m}$ located at the sphere's center. Therefore, in the fixed dipole model, the field due to bead n is

$$\mathbf{H}_{\text{dip}}(\mathbf{x} - \mathbf{Y}^{(n)}) = \frac{1}{4\pi}\left(\frac{3\mathbf{m}\cdot(\mathbf{x} - \mathbf{Y}^{(n)})}{r^5}(\mathbf{x} - \mathbf{Y}^{(n)}) - \frac{\mathbf{m}}{r^3}\right) \tag{15}$$

with $r = |\mathbf{x} - \mathbf{Y}^{(n)}|$. The force on the point dipole $\mathbf{m}$ due to field $\mathbf{H}$ is given by [13]

$$\mathbf{F} = \mu_0 \nabla(\mathbf{m} \cdot \mathbf{H}). \tag{16}$$

Thus, for an ensemble of N spheres each having dipole moment $\mathbf{m}$, the resulting force on bead n due to the other beads is

$$\mathbf{F}^{(n)} = \mu_0 \nabla_{\mathbf{Y}^{(n)}} \left(\mathbf{m} \cdot \sum_{k=1, k\neq n}^{N} \mathbf{H}_{\text{dip}}(\mathbf{Y}^{(n)} - \mathbf{Y}^{(k)}) \right). \tag{17}$$

Note that in (17) a depleted summation necessary to avoid self-singular terms. The applied field, $\mathbf{H}_0$, itself does not exert any force on the beads since the gradient of this field is zero.

2.2. Mutual dipole model

In the fixed-dipole model, only the external field was considered in the calculation of the dipole moments of the beads. The mutual dipole model allows for the fields of the other beads to contribute to the magnetization of the bead under consideration. This model is equivalent to providing a solution of the N-sphere problem with spherical harmonic expansions truncated at the dipole level, $L = 1$. Therefore, each sphere behaves as though isolated and immersed in a field whose strength is equal the sum of the external field and the fields due to the other beads evaluated at the sphere's center. Consequently, the dipole moment of bead n is

$$\mathbf{m}^{(n)} = \frac{4}{3}\pi a^3 \chi_{\text{eff}} \left(\mathbf{H}_0 + \sum_{k=1, k\neq n}^{N} \mathbf{H}^{(k)}_{\text{dip}}(\mathbf{Y}^{(n)} - \mathbf{Y}^{(k)}) \right). \tag{18}$$

In (18), the field $\mathbf{H}^{(k)}_{\text{dip}}$ is provided by (15) with dipole moment $\mathbf{m} = \mathbf{m}^{(k)}$. The dipole moments are unknown quantities and Eqs. (15) and (18) provide the $3N \times 3N$ linear system of equations needed to determine the dipole moments. Once the dipole moments have been found the force on sphere n is then

$$\mathbf{F}^{(n)} = \mu_0 \nabla_{\mathbf{Y}^{(n)}} \left(\mathbf{m}^{(n)} \cdot \sum_{k=1, k\neq n}^{N} \mathbf{H}^{(k)}_{\text{dip}}(\mathbf{Y}^{(n)} - \mathbf{Y}^{(k)}) \right). \tag{19}$$

To discuss the accuracy of the fixed and mutual dipole models, we compare the force between two spheres in a uniform field given by these models with the exact solution. The exact solution is provided by the calculation described in Section 4. In Fig. 1(a), we plot the force as a function of separation distance with the applied field parallel to the line of centers. In Fig. 1(b), the applied field is perpendicular to the line of centers. In both of these two plots $\mu/\mu_0 = 2$ and $\chi = 1$. It should be noted that when the field is aligned with the line of centers, the force is attractive whereas when it is perpendicular, the force is repulsive. As one expects, the mutual dipole model performs better than the fixed dipole model. Both models, however, break down as the particles come into contact and the neglected higher multipoles become important. Figs. 2(a) and (b) show the same configurations with $\mu/\mu_0 = 5$. As compared with the $\mu/\mu_0 = 2$ cases, the difference in the force given by the dipole models and the exact calculation is much more severe at separations less than three radii.

Other examples involving sets of three particles or eight particles are discussed later in the paper.

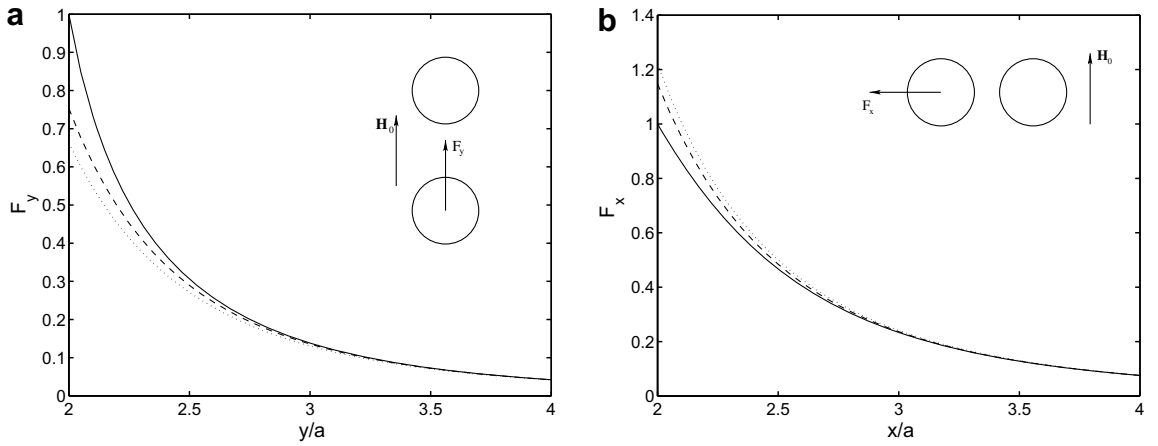

Fig. 1. Values of the interbead force for two beads in a uniform field $\mathbf{H_0} = (0, 1, 0)$ with $\mu/\mu_0 = 2$. (a) F_y as a function of separation. The values of F_y are normalized by the value of F_y of the exact solution at separation $y/a = 2$. (b) F_x as a function of separation. The values of F_x are normalized by the value of F_x of the exact solution at separation $x/a = 2$. The inset sketch is not drawn to scale and depicts the configuration of the beads relative to the applied field and the direction of the measured resulting force. In the plots: $(\cdots)$ fixed dipole; $(- - -)$ mutual dipole; $(—)$ exact solution.

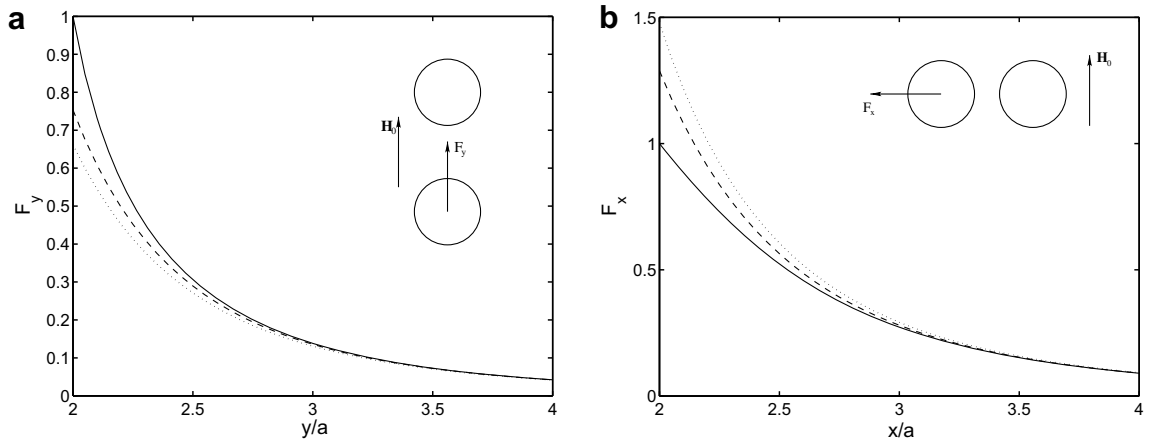

Fig. 2. Values of the interbead force for two beads in a uniform field $\mathbf{H_0} = (0, 1, 0)$ with $\mu/\mu_0 = 5$. (a) F_y as a function of separation. The values of F_y are normalized by the value of F_y of the exact solution at separation $y/a = 2$. (b) F_x as a function of separation. The values of F_x are normalized by the value of F_x of the exact solution at separation $x/a = 2$. The inset sketch is not drawn to scale and depicts the configuration of the beads relative to the applied field and the direction of the measured resulting force. In the plots: $(\cdots)$ fixed dipole; $(- - -)$ mutual dipole; $(—)$ exact solution.

3. Finite-dipole model

We have presented two dipole models commonly used to handle the magnetic interactions between paramagnetic beads. Both the fixed-dipole and mutual dipole models required an $O(N^2)$ pairwise calculation to determine the interparticle forces and to determine the dipole moments, in the case of the mutual dipole model. In this section, we present a new dipole model based on finite distributions of current density. Such a model is easily handled by many numerical techniques and readily adapts to confined geometries where boundary conditions on the magnetic field need to be imposed. Also, the finite nature of the resulting field eliminates the need for exclusive sums that are present in the other models due to the self-induced singular terms.

3.1. Finite-dipole model: single particle

To begin, we discuss how to represent a given magnetization by a distribution of current. First, consider a distribution of current density sources, **J**, in a vacuum. For this situation, Maxwell's equations are

$$\nabla \cdot \mathbf{B} = 0, \tag{20}$$

$$\nabla \times \mathbf{H} = \mathbf{J}, \tag{21}$$

$$\mathbf{B} = \mu_0 \mathbf{H}. \tag{22}$$

Eq. (20) allows us to introduce the vector potential, **A**, such that $\mathbf{B} = \nabla \times \mathbf{A}$. The choice of the Coloumb gauge, $\nabla \cdot \mathbf{A} = 0$, and the remaining two equations, (21) and (22), reveal

$$\nabla^2 \mathbf{A} = -\mu_0 \mathbf{J}. \tag{23}$$

Now, consider a system absent of any current sources, but where an induced magnetization, **M** is present. Here, Maxwell's equations give

$$\nabla \cdot \mathbf{B} = 0, \tag{24}$$

$$\nabla \times \mathbf{H} = \mathbf{0}, \tag{25}$$

$$\mathbf{B} = \mu_0(\mathbf{H} + \mathbf{M}). \tag{26}$$

We again introduce the vector potential, **A** and substitute the expression for **B** into the above equations and find

$$\nabla^2 \mathbf{A} = -\mu_0 \nabla \times \mathbf{M}. \tag{27}$$

By comparing (23) and (27), we can represent the magnetization **M** by a current distribution **J** by requiring $\mathbf{J} = \nabla \times \mathbf{M}$. The current density distribution associated with a point dipole located at the origin is [27]

$$\mathbf{J}_\delta(\mathbf{x}) = \nabla \times \mathbf{m}\delta(\mathbf{x}). \tag{28}$$

We wish to to remove the singularity while maintaining the localized nature of the distribution. To do this, we replace the Dirac delta function with a smoothly varying Gaussian function

$$\Delta(\mathbf{x}) = (2\pi\sigma^2)^{-3/2}\exp(-r^2/2\sigma^2). \tag{29}$$

Therefore, our current density is now

$$\mathbf{J}_\Delta = \nabla \times \mathbf{m}\Delta(\mathbf{x}) \tag{30}$$

and we are left with solving

$$\nabla^2\mathbf{A}_\Delta = -\mu_0\mathbf{J}_\Delta. \tag{31}$$

The solution to (31) is

$$\mathbf{A}_\Delta = \mu_0\frac{\mathbf{m}\times\mathbf{x}}{r}G'(r) \tag{32}$$

with the functions $G(r)$ and its derivative $G\prime(r)$ given by, see [28],

$$G(r) = -\frac{1}{4\pi r}\operatorname{erf}\left(\frac{r}{\sigma\sqrt{2}}\right), \tag{33}$$

$$G'(r) = \frac{1}{4\pi r^2}\left[\operatorname{erf}\left(\frac{r}{\sigma\sqrt{2}}\right) - \left(\frac{r}{\sigma}\right)\left(\frac{2}{\pi}\right)^{1/2}\exp(-r^2/2\sigma^2)\right]. \tag{34}$$

Rewriting (32) as

$$\mathbf{A} = \mu_0\mathbf{m}\times\nabla G \tag{35}$$

and using the fact that $\nabla^2 G = \Delta(\mathbf{x})$, the magnetic field $\mathbf{H} = \nabla\times\mathbf{A}/\mu_0$ is then evaluated as,

$$\mathbf{H}_\Delta(\mathbf{x}) = \mathbf{m}\Delta(\mathbf{x}) - \nabla(\mathbf{m}\cdot\nabla G(r)) \tag{36}$$

or, explicitly,

$$\mathbf{H}_\Delta(\mathbf{x}) = \frac{1}{4\pi}\left(\frac{3\mathbf{m}\cdot\mathbf{x}}{r^5}\mathbf{x} - \frac{\mathbf{m}}{r^3}\right)\operatorname{erf}\left(\frac{r}{\sigma\sqrt{2}}\right) + \left[\left(\mathbf{m} - \frac{\mathbf{m}\cdot\mathbf{x}}{r^2}\mathbf{x}\right) + \left(\mathbf{m} - \frac{3\mathbf{m}\cdot\mathbf{x}}{r^2}\mathbf{x}\right)\left(\frac{\sigma}{r}\right)^2\right]\Delta(\mathbf{x}). \tag{37}$$

In (37), the second term decays exponentially fast, and the dipole field is achieved once r/σ is large enough that $\operatorname{erf}(r/\sigma\sqrt{2})$ is close to one. The vector potential contours associated with (37) and those corresponding to a point dipole are depicted in Fig. 3. We notice the finite-dipole current distribution smoothes out the field in the region near the origin. Physically, the finite-dipole current distribution can be thought of as a current loop whose finite radius is represented by the size of the Gaussian envelope, σ.

Since this model is to be applied to particles of finite size, the ratio of a/σ will determine how well the field just outside the bead is resolved. In Fig. 4(a) and (b), we compare profiles of the magnetic field generated by finite-dipole current distributions of different σ with those of a point dipole field. Naturally, the approximation of the point dipole improves as we decrease the size of the Gaussian envelope, with the size ratio $a/\sigma = 4$ resolving nearly all the field at any distance from the surface of the sphere. Also, we observe the resolution of the field along the x-axis for a given a/σ is worse than along the y-axis.

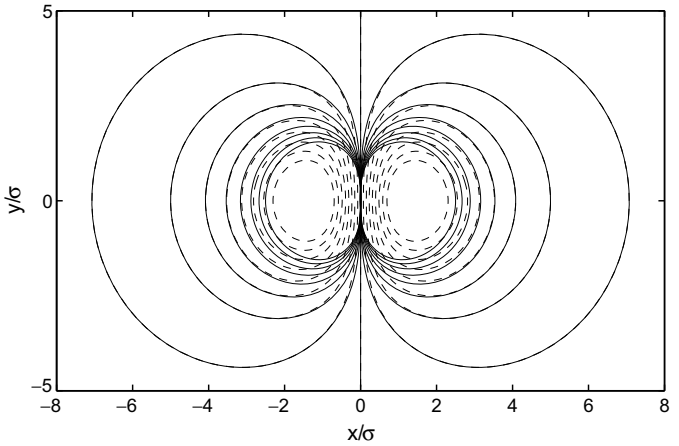

Fig. 3. Vector potential contours for a point dipole (—) and a finite-dipole current distribution (– – –) with $\sigma = 1$. In both cases $\mathbf{m} = (0, 1, 0)$.

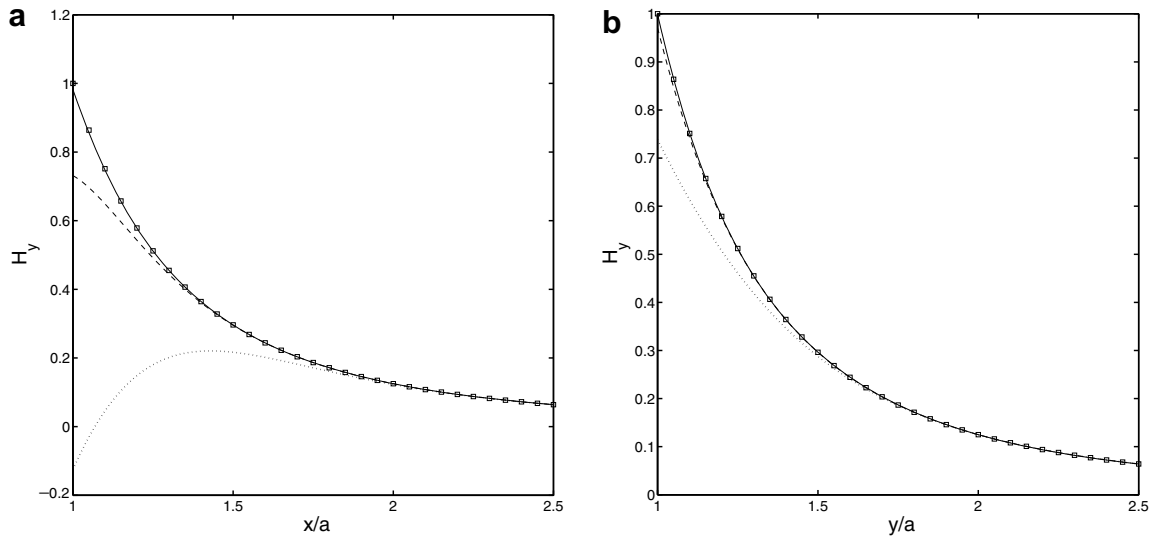

Fig. 4. Profiles of H_y for an isolated bead with $\mathbf{m} = 4\pi\chi a^3\mathbf{H_0}/3$, $\mathbf{H_0} = (0,1,0)$, and $\chi = 1$. (a) H_y along the x-axis where the values of H_y are normalized by the value of H_y of the true dipole at $x/a = 1$. (b) H_y along the y-axis with the values of H_y normalized by the value of H_y of the true dipole at $x/a = 1$. In the plots: $(\cdots)$ $a/\sigma = 2$; $(- - -)$ $a/\sigma = 3$; $(-)$ $a/\sigma = 4$; $(\square)$ point dipole.

3.2. Mutual finite-dipole model

So far, we have presented the representation of a single dipole from a finite distribution of current. Based on these results, we now formulate an iterative method to compute the magnetic interactions of a collection of paramagnetic spheres. First, suppose the beads have initial dipole moments $\mathbf{m}_0^{(n)}$ for $n = 1,\ldots,N$. These initial dipole moments may be those due to the external field or those from a previous timestep or iteration. Now, to motivate the method, we recall (18) and rewrite it as

$$\mathbf{m}^{(n)} = \frac{4}{3}\pi a^3\chi_{\text{eff}}\left(\mathbf{H}_0 + \sum_{k=1,k\neq n}^{N}\int \mathbf{H}_{\text{dip}}^{(k)}(\mathbf{x}-\mathbf{Y}^{(k)})\delta(\mathbf{x}-\mathbf{Y}^{(n)})\,\mathrm{d}^3\mathbf{x}\right). \tag{38}$$

In the mutual finite-dipole model, the dipole moment of bead n is given by

$$\mathbf{m}^{(n)} = \frac{4}{3}\pi a^3\chi_{\text{eff}}\left(\mathbf{H}_0 + \sum_{k=1,k\neq n}^{N}\int \mathbf{H}_{\Delta}^{(k)}(\mathbf{x}-\mathbf{Y}^{(k)})\Delta(\mathbf{x}-\mathbf{Y}^{(n)})\,\mathrm{d}^3\mathbf{x}\right). \tag{39}$$

In (39), the fields of the other beads are induced by moments $\mathbf{m}_0^{(n)}$ and given by (37). As a result everything on the right hand side of (39) is known. Also, the delta-function in the convolution is replaced by the Gaussian distribution (29). Therefore, rather than using the value of the field at a particle's center, a locally spatially averaged value of the field is considered in the computation of that particle's dipole moment.

In contrast to a singular point dipole, the field of a finite-dipole is finite and well defined at the dipole's location. We may then write

$$\mathbf{m}^{(n)} = \frac{4}{3}\pi a^3\chi_{\text{eff}}\left(\int (\mathbf{H}_{\text{tot}}(\mathbf{x}) - \mathbf{H}_{\Delta}^{(n)}(\mathbf{x}-\mathbf{Y}^{(n)}))\Delta(\mathbf{x}-\mathbf{Y}^{(n)})\,\mathrm{d}^3\mathbf{x}\right), \tag{40}$$

where

$$\mathbf{H}_{\text{tot}}(\mathbf{x}) = \mathbf{H}_0 + \sum_{k=1}^{N}\mathbf{H}_{\Delta}^{(k)}(\mathbf{x}-\mathbf{Y}^{(k)}). \tag{41}$$

Since the volume average of a particle's own field is

$$\int \mathbf{H}_{\Delta}^{(n)}(\mathbf{x}-\mathbf{Y}^{(n)})\Delta(\mathbf{x}-\mathbf{Y}^{(n)})\,\mathrm{d}^3\mathbf{x} = \frac{\mathbf{m}_0^{(n)}}{12(\pi\sigma^2)^{3/2}}, \tag{42}$$

we arrive at

$$\mathbf{m}^{(n)} = \frac{4}{3}\pi a^3\chi_{\text{eff}}\left(\int \mathbf{H}_{\text{tot}}(\mathbf{x})\Delta(\mathbf{x}-\mathbf{Y}^{(n)})\,\mathrm{d}^3\mathbf{x} - \frac{\mathbf{m}_0^{(n)}}{12(\pi\sigma^2)^{3/2}}\right). \tag{43}$$

Using the finite current density representation, the force on bead n is

$$\mathbf{F}^{(n)} = \mu_0 \int \mathbf{J}_{\Delta}^{(n)} \times (\mathbf{H}_{\text{tot}} - \mathbf{H}_{\Delta}^{(n)}(\mathbf{x} - \mathbf{Y}^{(n)})\, \mathrm{d}^3\mathbf{x}. \tag{44}$$

We may eliminate the need to subtract the self-induced forces since, in fact,

$$\int \mathbf{J}_{\Delta}^{(n)} \times \mathbf{H}_{\Delta}^{(n)}\, \mathrm{d}^3\mathbf{x} = 0. \tag{45}$$

Therefore, the force on bead n is simply

$$\mathbf{F}^{(n)} = \mu_0 \int \mathbf{J}_{\Delta}^{(n)} \times \mathbf{H}_{\text{tot}}\, \mathrm{d}^3\mathbf{x}. \tag{46}$$

Summarizing the above results, the numerical procedure with the mutual finite-dipole model is as follows:

(1) Using the values of the dipole moments from a previous timestep or iteration, $\mathbf{m}_0^{(n)}$ for $n = 1, \ldots, N$, construct the current density distribution $\sum_{n=1}^{N} \mathbf{J}_{\Delta}(\mathbf{x} - \mathbf{Y}^{(n)})$.
(2) Solve $\nabla^2 \mathbf{A} = -\mu_0 \sum_{n=1}^{N} \mathbf{J}_{\Delta}(\mathbf{x} - \mathbf{Y}^{(n)})$ for the vector potential $\mathbf{A}$ and compute $\mathbf{H} = \nabla \times \mathbf{A}/\mu_0$.
(3) Determine the new dipole moments

$$\mathbf{m}_n = \frac{4}{3}\pi a^3 \chi_{\text{eff}} \left(\int \mathbf{H}(\mathbf{x}) \Delta(\mathbf{x} - \mathbf{Y}^{(n)})\, \mathrm{d}^3\mathbf{x} - \frac{\mathbf{m}_0^{(n)}}{12(\pi\sigma^2)^{3/2}} \right) \tag{47}$$

for $n = 1, \ldots, N$.
(4) Check dipole moments for convergence. If $|\mathbf{m}^{(n)} - \mathbf{m}_0^{(n)}| > \epsilon$ then set $\mathbf{m}_0^{(n)} = \mathbf{m}^{(n)}$ and go to Step 1.
(5) If $|\mathbf{m}^{(n)} - \mathbf{m}_0^{(n)}| < \epsilon$ then evaluate the forces on the beads

$$\mathbf{F}^{(n)} = \mu_0 \int \mathbf{J}_{\Delta}(\mathbf{x} - \mathbf{Y}^{(n)}) \times \mathbf{H}(x)\, \mathrm{d}^3\mathbf{x} \tag{48}$$

for $n = 1, \ldots, N$.

The scheme described above can be implemented in variety of ways depending on the number of particles and the boundary conditions. For isolated configurations of few particles, one can construct a local grid for each particle and with the results (31) and (32) compute the integrals in steps (3) and (5). This method will, however, scale computationally as $O(N^2)$. In situations where many particles need to be considered, or boundaries are present, a fixed mesh over the entire domain can be constructed and a numerical solution for the vector potential (step (2)) can be determined. The integrals in steps (3) and (5) can then be computed using values of $\mathbf{H}_{\text{tot}}$ on nearby mesh points. The cost of computing the total magnetic field can be considered fixed. The cost of an additional particle is associated with the additional source term and the extra dipole and force integrations, which results in a method that scales computationally as $O(N)$. With the fixed mesh approach, there is the restriction that the grid spacing be small enough compared to the characteristic length scale of the distribution, σ as discussed in the following paragraph.

In order to analyze the how well the mutual finite-dipole model represents the mutual dipole model, we consider first two interacting spheres in a uniform magnetic field. In Fig. 5(a), we plot the dipole moments from the mutual dipole method and the mutual finite-dipole model using several different values of a/σ with the applied field perpendicular to the axis of separation. Fig. 5(b) shows the dipole moments when the field is parallel to the line of centers. Fig. 6(a) and (b) show the force computed from (46) as a function of separation for the perpendicular field and the parallel field respectively. Provided the finite current distributions are sufficiently localized, the dipole moments and the forces for both configurations are nearly identical to those given by the mutual dipole method. We also notice that even though the field near the surface of a sphere is not fully resolved when $a/\sigma = 3$, the particle interactions are well accounted for. The results presented here are for $\mu/\mu_0 = 2$. Higher permeability ratios were also considered but not plotted here since the relative error for a choice of a/σ is not affected by this ratio.

Additionally, we have considered how well the mutual finite-dipole model recovers the dipolar interactions in a linear chain of particles. In this example, successive particles are in contact and the chain is aligned with the applied field, with $\mu/\mu_0 = 2$ or $\chi = 1$. Table 1 shows the dipole moments for each bead in the chain for a range of values for a/σ. For values of $a/\sigma \geqslant 2$ the resulting dipole moments compare well with those given by the mutual dipole model. To obtain an accurate quantification of magnetic force on each bead, see Table 2, requires a more localized distribution with values of $a/\sigma > 2.5$ yielding good estimates. It should be noted that the mutual dipole model underestimates the actual interaction forces between the particles due to the neglect of higher-order interaction effects. This is discussed in the next section.

In the force-coupling method (FCM) [28], the ratio a/σ is chosen to exploit the self-induced velocity of a particle subject to an external body force by matching the local spatial average of this field to the settling velocity of the particle. This specific choice further gives the proper balance between the work done on the fluid and the viscous dissipation. For the mutual finite-dipole model, the self-induced moment can not be exploited and must, in fact, be removed. As a result, there is no

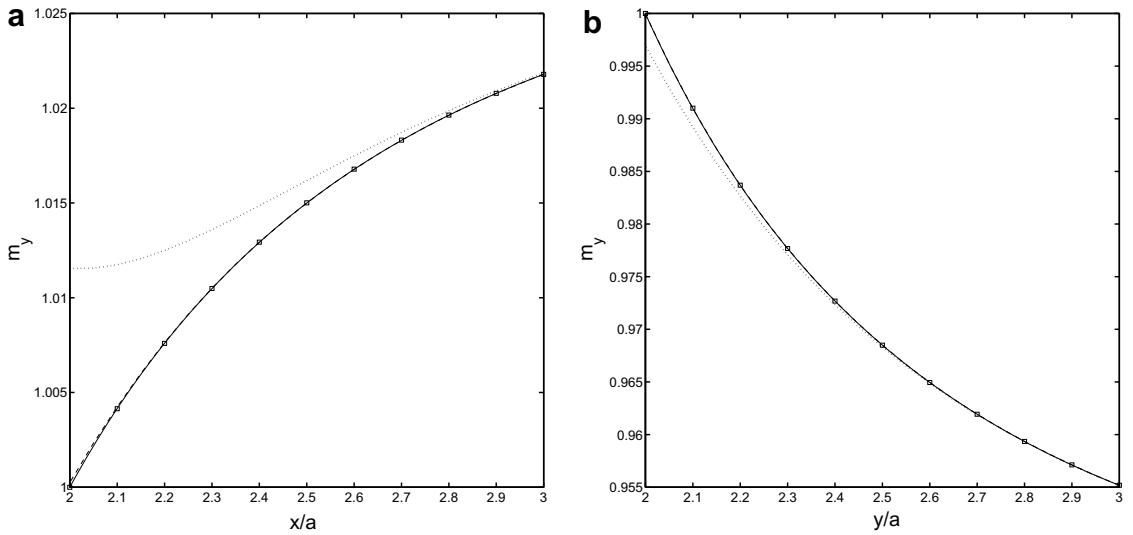

Fig. 5. Values of m_y as a function of separation for two beads in a uniform field $\mathbf{H_0} = (0, 1, 0)$ and $\mu/\mu_0 = 2$. (a) Separation along the x-axis. The values of m_y are normalized by the value of m_y of the mutual dipole at separation $x/a = 2$. (b) Separation along the y-axis. The values of m_y are normalized by the value of m_y of the mutual dipole at separation $y/a = 2$. In the plots: $(\cdots)$ $a/\sigma = 2$; $(- - -)$ $a/\sigma = 3$; $(-)$ $a/\sigma = 4$; $(\square)$ point dipole.

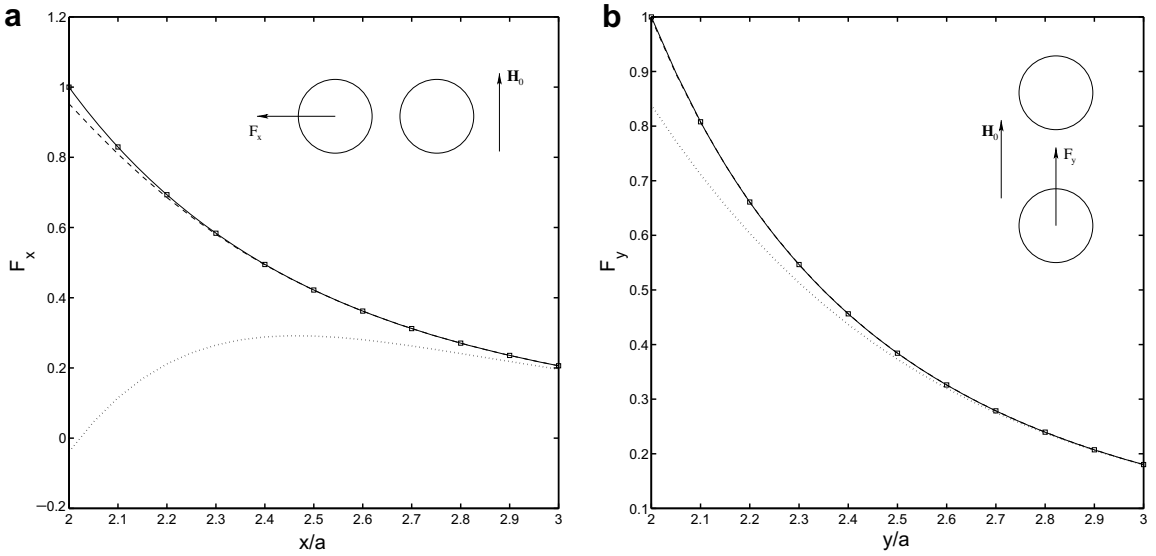

Fig. 6. Values of interparticle force for two beads in a uniform field $\mathbf{H_0} = (0, 1, 0)$ and $\mu/\mu_0 = 2$. (a) The values of F_x as a function of separation normalized by the value of F_x of the mutual dipole at separation $x/a = 2$. (b) Values of F_y versus separation normalized by the value of F_y of the mutual dipole at separation $y/a = 2$. The inset sketch is not drawn to scale and depicts the configuration of the beads relative to the applied field and the direction of the measured resulting force. In the plots: $(\cdots)$ $a/\sigma = 2$; $(- - -)$ $a/\sigma = 3$; $(-)$ $a/\sigma = 4$; $(\square)$ point dipole.

Table 1
The magnitude of the magnetic dipole moment, $|\mathbf{m}|$, for each bead in an eight-bead chain with the chain axis aligned with the applied field, $|\mathbf{H}_0| = 1$ and $\chi = 1$

Bead	Mutual dipole	$a/\sigma = 3/2$	$a/\sigma = 2$	$a/\sigma = 5/2$	$a/\sigma = 3$
1	3.412583	3.358042	3.400500	3.411038	3.412467
2	3.627707	3.524409	3.604898	3.624793	3.627488
3	3.667280	3.558145	3.643083	3.664185	3.667074
4	3.677247	3.566890	3.652764	3.674115	3.677012

The dipole moments are computed using the mutual dipole method and the finite-dipole method with various values of a/σ.

Table 2
The magnetic forces, F/μ_0, on each bead in an eight-bead chain with the chain axis aligned with the applied field, $|\mathbf{H}_0| = 1$ and $\chi = 1$

Bead	Mutual dipole	$a/\sigma = 3/2$	$a/\sigma = 2$	$a/\sigma = 5/2$	$a/\sigma = 3$
1	0.399889	0.212705	0.338805	0.388854	0.398762
2	0.059832	0.041282	0.053863	0.058807	0.059732
3	0.014335	0.010425	0.013117	0.014129	0.014315
4	0.003119	0.002323	0.002874	0.003078	0.003115

The forces are computed using the mutual dipole method and the finite-dipole method with various values of a/σ.

preferred choice of a/σ and its value may be chosen for numerical accuracy or efficiency. As a/σ increases, the dipole moments and the forces given by the finite-dipole model become more accurate, however, the spatial grid size must decrease to resolve the more localized Gaussian. The goal is to choose a value that correctly reproduces the point dipole interactions up to a certain distance but requires a reasonable number of grid points per particle radius. In the previous section, we saw that the force computed using the mutual dipole model begins to diverge from the exact calculation at a separation of three radii. With values $a/\sigma = 2.5$—3.0, the mutual finite-dipole model resolves the force at this separation. Also, with this range of values of a/σ, the resulting dipole moments agree quite well with the mutual dipole model at any separation. This is important for the inclusion of higher multipoles to be effective when using the procedure that will be described in Section 4.2.

3.3. Computational effort

In the standard mutual dipole model, the number of equations in (18) grows as the number of particles increases. An advantage of the finite-dipole model is its computational scalability. To include additional beads, one needs only to add the associated current density distribution of the extra bead to the equation for the vector potential. To illustrate how the computational cost increases as we increase the number of particles, we conducted several simulations of the aggregation of paramagnetic beads from a homogeneous random suspension in response to an external magnetic field. In addition to the magnetic forces we include hydrodynamic and solid-body contact forces. The Reynolds number associated with the motion of these particles is low, $Re \approx 10^{-4}$, and the density of the particles is close to the density of the surrounding fluid, $\rho_p \approx \rho_f$. At each instant of time, the forces on each particle must balance

$$\mathbf{F}^{(n)}_{\text{hydro}} + \mathbf{F}^{(n)}_{\text{mag}} + \mathbf{F}^{(n)}_{\text{bar}} = \mathbf{0}. \tag{49}$$

A short-range, pairwise barrier force between particles is included to represent solid-body contact. The force on particle-n from particle-m is zero if the distance between the particle centers $r_{nm} = |\mathbf{x}_{nm}|$, where $\mathbf{x}_{nm} = \mathbf{Y}^{(n)} - \mathbf{Y}^{(m)}$, exceeds a cut-off distance R_{ref}. For shorter separations, the barrier force is of the form

$$\mathbf{F}^{\text{bar}}_{nm} = -\frac{F_{\text{ref}}}{2a}\left(\frac{R^2_{\text{ref}} - r^2_{nm}}{R^2_{\text{ref}} - 4a^2}\right)^4 \mathbf{x}_{nm}. \tag{50}$$

The force balance (49) establishes a low Reynolds number mobility problem where, after determining the magnetic and barrier forces, the motion of the fluid and the particles is computed using FCM. In FCM, the forces the particle phase exerts on the fluid are represented by a finite force multipole expansion in the Stokes equation, see [28,29],

$$\nabla p - \eta\nabla^2\mathbf{u} = \sum_{n=1}^{N} \mathbf{F}^{(n)}_{\text{ext}} \Delta_{\text{FCM}}(\mathbf{x} - \mathbf{Y}_n), \tag{51}$$

$$\nabla \cdot \mathbf{u} = 0, \tag{52}$$

where $\mathbf{F}^{(n)}_{\text{ext}} = \mathbf{F}^{(n)}_{\text{mag}} + \mathbf{F}^{(n)}_{\text{bar}}$ and Δ_{FCM} is a Gaussian envelope, with the length scale σ_{FCM} set as $a/\sigma_{\text{FCM}} = \sqrt{\pi}$. Aside from the evaluation of the magnetic forces, these procedures are similar to those used previously [18].

In this simulation, the boundary conditions in each direction are periodic so a Fourier collocation method with 144^3 grid points is used to solve for the magnetic vector potential. The hydrodynamic interactions are given by FCM and a Fourier collocation method with 96^3 grid points provides the solution to the Stokes equations. A different grid spacing is used for the magnetic field as opposed to the flow field since the length scale of the Gaussian in the finite-dipole model is two-thirds that of FCM. As the barrier forces vanish beyond separation distances of R_{ref}, a linked list algorithm is employed to handle efficiently the pairwise interactions. The simulation is run for 100 timesteps on two 2.4 GHz Intel Xeon processors and the time needed to update the dipole moments is recorded. In the finite-dipole computations, it typically required 2–3 iterations per timestep for the magnetic dipole moments to converge. This time is plotted in Fig. 7. When there are few particles, the simulation time remains constant as the time required to distribute the current sources on the grid is less than the fixed time associated with solving the equations. In this regime, a point dipole approach may be computationally advantageous as the cost of solving the Poisson equations is likely to exceed the cost of building and solving the $3N \times 3N$ linear system of equations to determine the dipole moments. As we increase the number of beads, however, the computational time required to distribute the sources exceeds the solve time and we observe that the computational work scales as $O(N)$. It is these

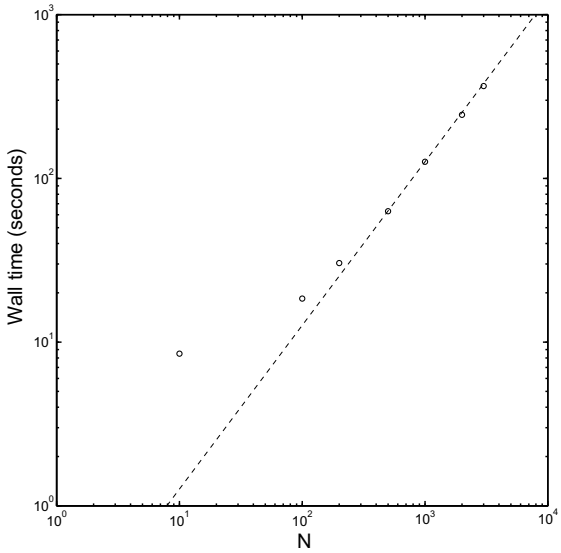

Fig. 7. Computational time for one hundred time steps ($T = 100\Delta t$) associated with the mutual finite-dipole model as a function of the number of beads. (∘) measured wall time; (– – –) O(N).

situations where large numbers of particles are involved, employing the finite-dipole is appropriate and can out perform traditional point dipole methods.

4. Incorporating higher multipoles

Until now, we have discussed various dipole models to account for the magnetic interactions of paramagnetic beads. As shown in Fig. 1(a) and (b), the dipole models provide reliable estimates for the inter-particle forces at larger separation distances but become inaccurate when the gap between particles is less than half a radius. In this section, we present the exact two-body calculation for the pairwise interaction of particles. The results will be then used to include the effects of higher-order multipole terms in a refined dipole model.

4.1. Solution to the two-body problem

Consider the general problem described in Section 2 with $N = 2$, $\mathbf{Y}^{(1)} = (0, 0, c)$, $\mathbf{Y}^{(2)} = (0, 0, 0)$ and the applied magnetic field resolved into components parallel to and orthogonal to the line of centers, $\mathbf{H}_0 = H_\perp \hat{\mathbf{x}} + H_\parallel \hat{\mathbf{z}}$. The problem is depicted in Fig. 8 and is based on that performed in [30]. It is also a specific case considered in [15]. As stated earlier, the solution to this problem is given by a sum of spherical harmonics. For this problem we have

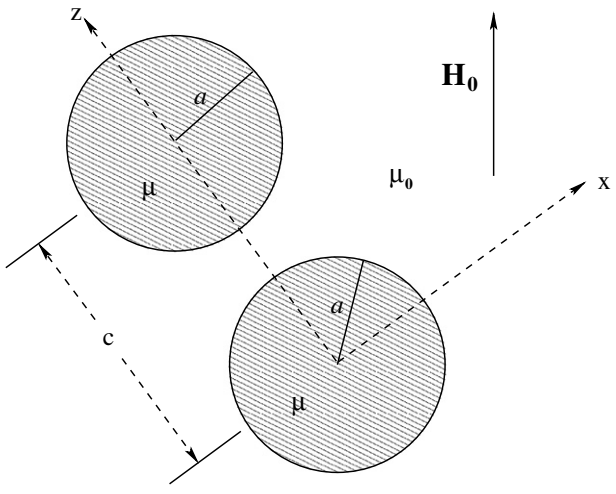

Fig. 8. The two body problem.

$$\Phi_{\text{in}}^{(n)} = \sum_{l=0}^{\infty}\sum_{m=0}^{1}\alpha_{lm}^{(n)} r_n^l P_l^m(\cos\theta_n)\cos m\phi, \tag{53}$$

$$\Phi_{\text{out}} = -H_\perp x - H_\parallel z + \sum_{n=1}^{2}\sum_{l=0}^{\infty}\sum_{m=0}^{1}\beta_{lm}^{(n)}\frac{P_l^m(\cos\theta_n)}{r_n^{l+1}}\cos m\phi, \tag{54}$$

where (r_n, θ_n, ϕ) are the spherical coordinates of a system whose origin coincides with the center of sphere n. The associated Legendre functions are defined as

$$P_l^m(\cos\theta) = (-1)^m(1-\cos^2\theta)^{m/2}\frac{\mathrm{d}^m}{\mathrm{d}(\cos\theta)^m}P_l(\cos\theta). \tag{55}$$

In order to find the coefficients $\alpha_{lm}^{(n)}$ and $\beta_{lm}^{(n)}$ that satisfy boundary conditions (7) and (8), we must express the general solution in terms of a single coordinate system. To accomplish this task, we employ the Hobson formula [30,15] which state

$$\frac{P_l^m(\cos\theta_1)}{r_1^{l+1}} = \sum_{s=m}^{\infty}(-1)^{s+m}(-1)^{l+s}\binom{l+s}{s+m}\frac{r_2^s}{c^{l+s+1}}P_s^m(\cos\theta_2), \tag{56}$$

$$\frac{P_l^m(\cos\theta_2)}{r_2^{l+1}} = \sum_{s=m}^{\infty}(-1)^{s+m}\binom{l+s}{s+m}\frac{r_1^s}{c^{l+s+1}}P_s^m(\cos\theta_1). \tag{57}$$

On substituting the general solution into the boundary conditions, applying the Hobson formula, and eliminating $\alpha_{lm}^{(n)}$ we find that for each $m = 0, 1$

$$\left(\frac{\mu}{\mu_0}l + l + 1\right)\beta_{lm}^{(1)} + \sum_{s=1}^{\infty}\beta_{sm}^{(2)}(-1)^{l+m}\binom{l+s}{s+m}\frac{a^{2l+1}}{c^{l+s+1}}\left(\frac{\mu}{\mu_0}l - l\right) = \delta_{1j}a^3\left(1-\frac{\mu}{\mu_0}\right)(\delta_{1m}H_\perp - \delta_{0m}H_\parallel), \tag{58}$$

$$\left(\frac{\mu}{\mu_0}l + l + 1\right)\beta_{lm}^{(2)} + \sum_{s=1}^{\infty}\beta_{sm}^{(1)}(-1)^{l+s}(-1)^{l+m}\binom{l+s}{s+m}\frac{a^{2l+1}}{c^{l+s+1}}\left(\frac{\mu}{\mu_0}l - l\right) = \delta_{1j}a^3\left(1-\frac{\mu}{\mu_0}\right)(\delta_{1m}H_\perp - \delta_{0m}H_\parallel). \tag{59}$$

By including only a finite number of multipoles, $l = 0, \ldots, L$, (58) and (59) establish two $2L \times 2L$ linear systems of equations. Specifically, for each $m = 0, 1$ we need to solve

$$\left(\begin{array}{c|c} \mathbf{X} & \boldsymbol{\Delta}_m \\ \hline \boldsymbol{\Gamma}_m & \mathbf{X} \end{array}\right)\left(\begin{array}{c} \boldsymbol{\beta}_m^{(1)} \\ \hline \boldsymbol{\beta}_m^{(2)} \end{array}\right) = \left(\begin{array}{c} \mathbf{q}_m \\ \hline \mathbf{q}_m \end{array}\right) \tag{60}$$

where

$$\boldsymbol{\beta}_m^{(1)} = (\beta_{1m}^{(1)}, \beta_{2m}^{(1)}, \ldots, \beta_{Lm}^{(1)})^{\mathrm{T}}, \tag{61}$$

$$\boldsymbol{\beta}_m^{(2)} = (\beta_{1m}^{(2)}, \beta_{2m}^{(2)}, \ldots, \beta_{Lm}^{(2)})^{\mathrm{T}}, \tag{62}$$

$$\mathbf{q}_0 = (H_\parallel a^3(1-\mu/\mu_0), 0, \ldots, 0)^{\mathrm{T}}, \tag{63}$$

$$\mathbf{q}_1 = (-H_\perp a^3(1-\mu/\mu_0), 0, \ldots, 0)^{\mathrm{T}} \tag{64}$$

and the $L \times L$ matrices are

$$X_{ij} = \delta_{ij}\left(i\frac{\mu}{\mu_0} + i + 1\right), \tag{65}$$

$$\Delta_{ij;m} = (-1)^{i+m}\left(i\frac{\mu}{\mu_0} - i\right)\binom{i+j}{j+m}\frac{a^{2i+1}}{c^{i+j+1}}, \tag{66}$$

$$\Gamma_{ij;m} = (-1)^{i+j}\Delta_{ij;m}. \tag{67}$$

After solving for the $\beta_{lm}^{(n)}$, the contribution of the field from the particles in the fluid is

$$H_r = \sum_{l=0}^{L}\sum_{m=0}^{1}\left[(l+1)\beta_{lm}^{(1)}\frac{P_l^m(\cos\theta_1)}{r_1^{l+2}} - \beta_{lm}^{(2)}\sum_{s=m}^{L}(-1)^{s+m}\binom{l+s}{s+m}s\frac{r_1^{s-1}}{c^{l+s+1}}P_s^m(\cos\theta_1)\right]\cos m\phi, \tag{68}$$

$$H_\theta = -\sum_{l=0}^{L}\sum_{m=0}^{1}\left[\frac{\beta_{lm}^{(1)}}{r_1^{l+2}}\frac{\mathrm{d}P_l^m(\cos\theta_1)}{\mathrm{d}\theta_1} + \beta_{lm}^{(2)}\sum_{s=m}^{L}(-1)^{s+m}\binom{l+s}{s+m}\frac{r_1^{s-1}}{c^{l+s+1}}\frac{\mathrm{d}P_s^m(\cos\theta_1)}{\mathrm{d}\theta_1}\right]\cos m\phi, \tag{69}$$

$$H_\phi = \sum_{l=0}^{L}\left[\frac{\beta_{l1}^{(1)}}{r_1^{l+2}\sin\theta_1}P_l^1(\cos\theta_1) + \beta_{l1}^{(2)}\sum_{s=1}^{L}(-1)^{s+1}\binom{l+s}{s+1}\frac{r_1^{s-1}}{c^{l+s+1}\sin\theta_1}P_s^1(\cos\theta_1)\right]\sin\phi. \tag{70}$$

In (68)–(70), the coordinate system is (r_1, θ_1, ϕ), but using the Hobson formula, the field can also be expressed in terms of (r_2, θ_2, ϕ). With the field known, the Maxwell stress tensor, (10), can be formed and the force is then

$$F_x = \int_{r_n=a} T_{xr}\, dS, \tag{71}$$

$$F_y = 0, \tag{72}$$

$$F_z = \int_{r_n=a} T_{zr}\, dS. \tag{73}$$

The simple form of the azimuthal dependence of the field allows the integration over ϕ to be evaluated analytically while the polynomial dependence of the field on $\cos\theta$ makes Gaussian integration viable for the integration over θ.

In the calculation, the infinite summation is truncated at a finite value, L. It is important that this value be large enough to include the important multipoles, but not so large that the matrix inversion becomes cumbersome. Fig. 9(a) and (b) show the value of the force as a function of L between two spheres in contact with the axis of separation parallel to the applied field with $\mu/\mu_0 = 2$ and $\mu/\mu_0 = 5$ respectively. When $\mu/\mu_0 = 2$, having $L = 10$ resolves nearly all the force where as a value of $L = 20$ is needed to provide the same level of accuracy if $\mu/\mu_0 = 5$.

4.2. Inclusion of two-body effects into dipole models

We have already seen that as two bodies come into contact, the various dipole models fail to give an accurate representation of the magnetic force between a pair of particles. We, therefore, would like to incorporate higher order multipoles to yield correct estimates of the near contact force. One way to accomplish this is to compute the pairwise interactions using a higher multipole representation of the interactions [23]. While computing the forces this way will give a more accurate estimation of the near contact force, this method will not produce the correct asymptotic results for a many-body problem where the particles are widely separated. Consequently, we seek to develop a method that blends an N-body dipole calculation to determine the many body interactions and two-body, higher multipole calculations between particles that are sufficiently close. Such a model will provide the necessary adjustments for the near contact interactions while preserving the correct far-field forces given by the dipole computation. The method we propose to include the near field magnetic interactions is described here considering an ensemble of N spheres each of permeability μ and radius a.

4.2.1. Step 1: Far-field/dipole calculation

First, one must perform the N-body dipole calculation obtaining the resulting dipole moments $\mathbf{m}^{(n)}$ and magnetic forces $\mathbf{F}^{(n)}_{\text{mag}}$ on each bead n. This computation can be handled using either the mutual dipole or the mutual finite-dipole method depending on the choice of the user. The procedure to include the higher order multipoles is general and available to both methods.

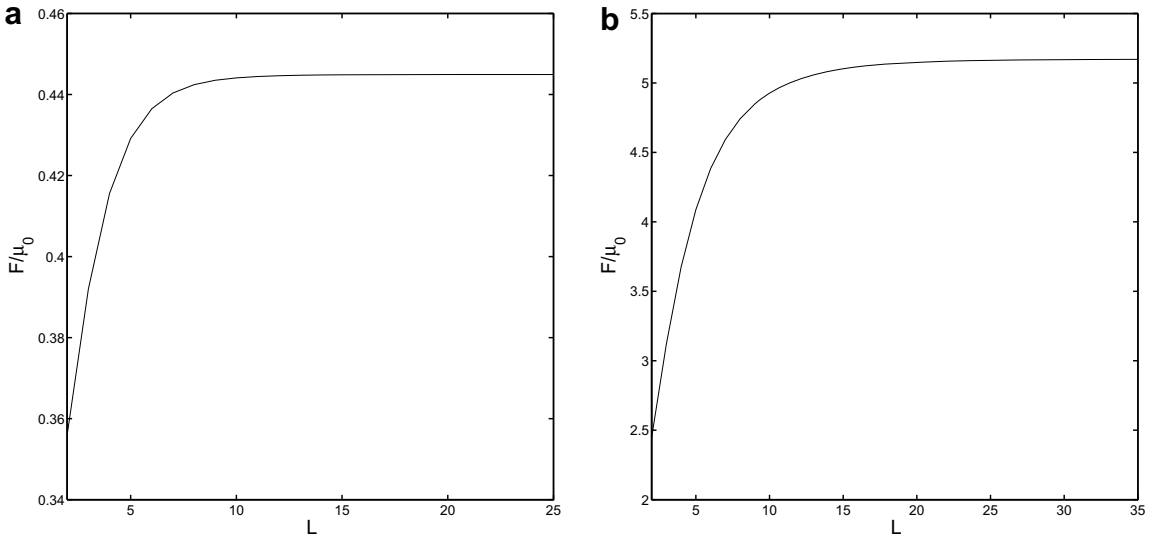

Fig. 9. Resulting attractive force as a function of the number of multipoles. The field is aligned with the line of centers and $|\mathbf{H_0}| = 1$. (a) $\mu/\mu_0 = 2$ and (b) $\mu/\mu_0 = 5$.

4.2.2. Step 2: Determine if $c < R_c$

Since higher multipoles become important only near contact, we introduce R_c which defines the maximum inter-bead separation distance where higher multipoles will be included in the force calculations. Therefore, after computing the dipole interactions, one must determine if a pair of particles are close enough such that higher multipoles should be considered. In our simulations this is handled using a linked list algorithm [31] to avoid pairwise checking over all N particles and checking if the separation distance $c = |\mathbf{Y}^{(p)} - \mathbf{Y}^{(q)}|$ is less than R_c.

4.2.3. Step 3: Compute higher order multipoles

For each pair whose separation distance is less than R_c we perform the two-body calculation (60) to determine the vectors $\boldsymbol{\beta}_m^{(1)}$ and $\boldsymbol{\beta}_m^{(2)}$ for $m = 0, 1$ which hold the coefficients for the L multipoles. In the two-body calculation, the axes are aligned such that

$$\hat{\mathbf{z}} = \frac{\mathbf{Y}^{(p)} - \mathbf{Y}^{(q)}}{c}, \tag{74}$$

$$\hat{\mathbf{x}} = \frac{\mathbf{H}_0 - (\mathbf{H}_0 \cdot \hat{\mathbf{z}})}{|\mathbf{H}_0 - (\mathbf{H}_0 \cdot \hat{\mathbf{z}})|}, \tag{75}$$

$$\hat{\mathbf{y}} = \hat{\mathbf{z}} \times \hat{\mathbf{x}}, \tag{76}$$

so

$$H_{\parallel} = \mathbf{H}_0 \cdot \hat{\mathbf{z}}, \tag{77}$$

$$H_{\perp} = \mathbf{H}_0 \cdot \hat{\mathbf{x}}. \tag{78}$$

This calculation can be performed on the fly at each time step, as needed, since only two $2L \times 2L$ linear systems need to be solved for each pair, and $L = 10$ for $\mu/\mu_0 = 2$ and $L = 20$ for $\mu/\mu_0 = 5$.

4.2.4. Step 4: Adjust two-body dipole moments to include far-field effects

Before computing the interparticle force, we first modify the dipole coefficients from the two-body calculations $\beta_{1m}^{(p),2B}$ and $\beta_{1m}^{(q),2B}$ to include far-field effects. This allows information from the far-field to influence the two-body force calculation. With the relations

$$\beta_{10}^{(n),\mathrm{dip}} = \frac{\mathbf{m}^{(n)} \cdot \hat{\mathbf{z}}}{4\pi a^3}, \tag{79}$$

$$\beta_{11}^{(n),\mathrm{dip}} = \frac{-\mathbf{m}^{(n)} \cdot \hat{\mathbf{x}}}{4\pi a^3} \tag{80}$$

we determine the new dipole coefficients

$$\beta_{1m}^{(n)} = \beta_{1m}^{(n),2B} + \beta_{1m}^{(n),\mathrm{dip}} - \beta_{1m}^{(n),2B\mathrm{dip}} \tag{81}$$

for each $m = 0, 1$. In (81), $\beta_{1m}^{(n),2B\mathrm{dip}}$ is given by a dipole calculation where only the interactions of the two bodies are considered. This value corresponds to the outer expansion of the inner solution and is the overlap of the two solutions that must be subtracted to avoid it being counted twice.

4.2.5. Step 5: Determine the resulting field

With the modified coefficients $\beta_{lm}^{(n)}$ we now determine the field in the fluid phase (68)–(70). In general, one needs to add the out of plane component of the field due to the out of plane component of the dipole moment from the far-field calculation

$$\mathbf{H} = -\nabla \Phi_y = -\frac{\mathbf{m}^{(n)} \cdot \hat{\mathbf{y}}}{4\pi a^3} \frac{P_1^1(\cos\theta)\sin\phi}{r^2}. \tag{82}$$

4.2.6. Step 6: Form and evaluate the Maxwell stress tensor

Once the components of the field are found, the Maxwell stress tensor (10) can be determined and evaluated over the surface of each particle to obtain the force (11), $\mathbf{F}_{\mathrm{mag}}^{(n),2B}$.

4.2.7. Step 7: Correct the total magnetic force

The total magnetic force on a given particle must now be adjusted to replace the magnetic force between particles p and q with the corrected force $\mathbf{F}_{\mathrm{mag}}^{(pq),2B}$. The total force is

$$\mathbf{F}^{(p)} = \mathbf{F}_{\mathrm{dip}}^{(p)} + \mathbf{F}_{2B}^{pq} - \mathbf{F}_{\mathrm{dip}2B}^{pq}, \tag{83}$$

$$\mathbf{F}^{(q)} = \mathbf{F}_{\mathrm{dip}}^{(q)} - \mathbf{F}_{2B}^{pq} + \mathbf{F}_{\mathrm{dip}2B}^{pq}, \tag{84}$$

where $\mathbf{F}_{\mathrm{dip}2B}^{pq}$ is the dipolar force between particles p and q.

4.3. Example results

To test the effectiveness of this procedure, we consider several three-particle configurations with different values of μ/μ_0. Two-particle problems are not considered since the inclusion procedure, described above, already gives exact results for the interparticle force. For the three-body problems, the interparticle forces are computed in turn from the mutual dipole method, a combination of simple pairwise two-body calculations [23] and the inclusion model. These results are compared to the exact forces. The results of the two-body calculation are obtained by summing the forces from the two-body calculation for each pair in turn [23]. Fig. 10(a) and (b) show the force on a bead due to a collinear pair of beads in contact. The axis of separation is aligned with the axis of the doublet pair and the applied magnetic field is taken in turn to be perpendicular and parallel to this direction. The magnetic susceptibility is $\chi = 1$ and $\mu/\mu_0 = 2$. For these axisymmetic configurations, we extend the two-body spherical harmonic calculation to determine the exact magnetic forces on three beads. For $\mu/\mu_0 = 2$, we used $L = 20$ multipoles in this computation. When the magnetic field is aligned with the axis of the three-particle chain the results of the inclusion model agree well with the exact values. In this configuration, the forces are attractive and the agreement indicates how well the models can characterize the yield behavior of the chain structures commonly found in MR fluids. When the field is perpendicular to the chain, the forces are repulsive and the particles tend to separate. The error from the inclusion model is small and is a significant improvement over the estimates from the other methods. In Fig. 11(a) and (b), the same bead configurations are used, but now $\mu/\mu_0 = 5$. Here, a $L = 30$ multipole calculation provided the exact force values.

The trends in the discrepancies in the differences between the models and the exact computations are the same for both permeability ratios but more dramatic in the case of $\mu/\mu_0 = 5$ where the higher multipoles are more influential. In each case, the mutual dipole method performed well at large separations, but diverged from the exact force near contact. Simply adding the forces from pairwise two-body calculations gives a better estimate of the force near contact and a good estimate at any separation when the chain axis is perpendicular to the applied field. This method does, however, suffer from not being able to provide an accurate characterization of the far-field force where the chain axis is aligned with the applied field. For the higher permeability ratio, the relative error at contact is still large at 15% (Fig. 11(b)). In each of these three-particle configurations and for both permeability ratios, we see the inclusion of the higher multipoles from the two-body calculation with the many-body dipole model provides the force enhancement needed to resolve the near contact interactions while also ensuring the proper asymptotic behavior as the separation increases. Of the four cases considered here, the largest relative error is approximately 5% (Fig. 11(b)).

The inclusion model may be applied to the example of a collinear chain of eight paramagnetic beads in contact, previously considered in Section 3.2, with the applied field aligned with the chain. The resultant magnetic forces on each particle in the chain are evaluated using the different methods and listed in Table 3. The results are compared to the exact values. The inclusion procedure provides a good quantification of the force on each particle resolving the underestimate associated with the

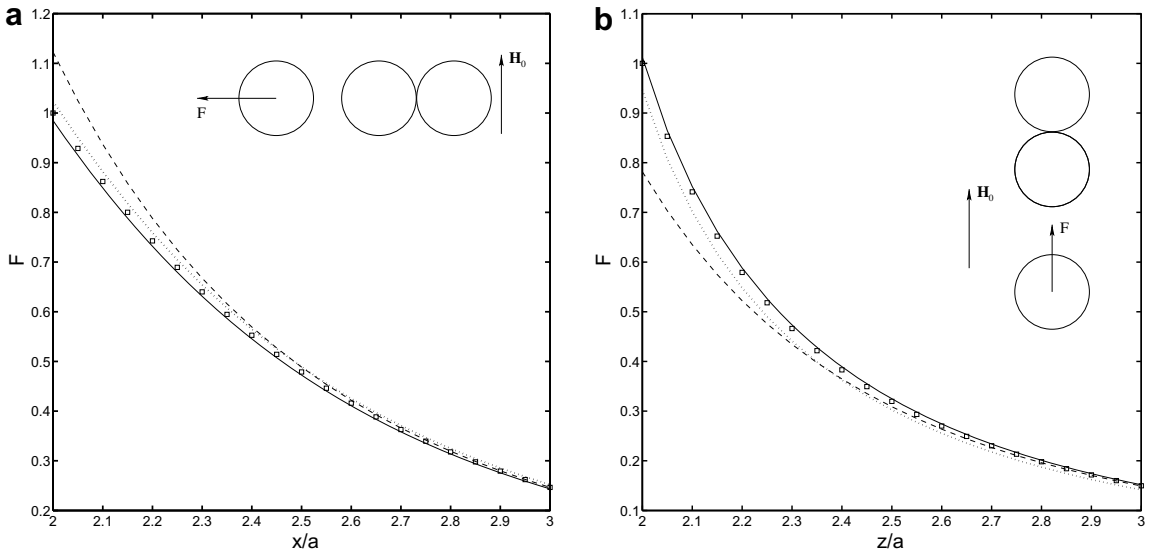

Fig. 10. Force on a bead due to a doublet with $\mu/\mu_0 = 2$. The data are normalized by the value of the exact solution at contact. (a) The applied field is perpendicular to the separation axis. (b) The applied field is parallel to the separation axis. The inset sketch is not drawn to scale and depicts the configuration of the beads relative to the applied field and the direction of the measured resulting force. In the plots: (···) two-body calculation; (– – –) mutual dipole; (—) inclusion model; (□) exact solution.

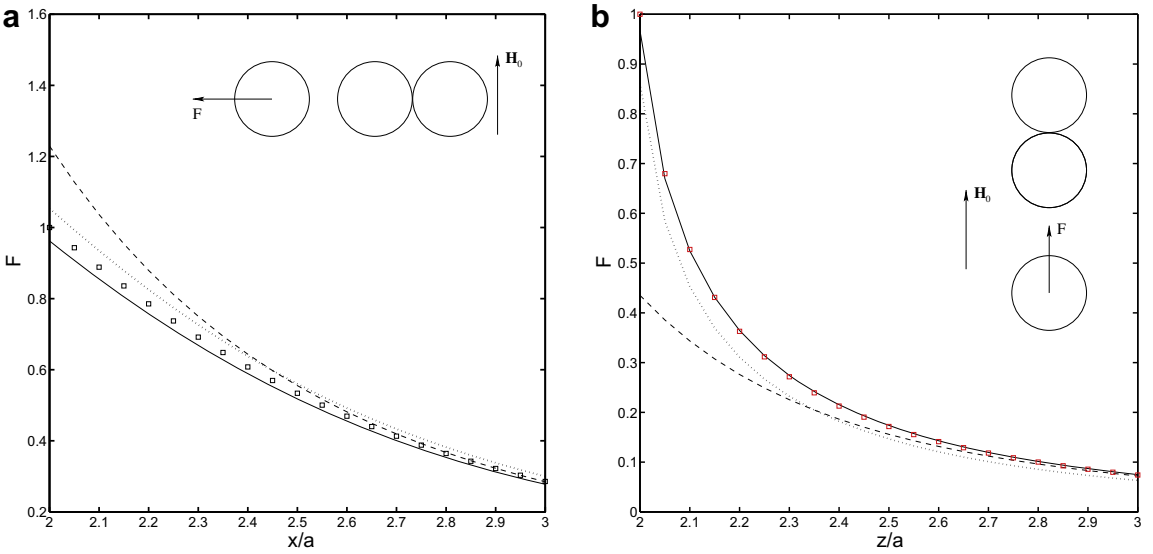

Fig. 11. Force on a bead due to a doublet with $\mu/\mu_0 = 5$. The data are normalized by the value of the exact solution at contact. (a) The applied field is perpendicular to the separation axis. (b) The applied field is parallel to the separation axis. The inset sketch is not drawn to scale and depicts the configuration of the beads relative to the applied field and the direction of the measured resulting force. In the plots: (···) two-body calculation; (– – –) mutual dipole; (—) inclusion model; (□) exact solution.

Table 3
The resultant magnetic forces, F/μ_0, on each bead in an eight-bead chain with the chain axis aligned with an applied field of unit magnitude, $|\mathbf{H}_0| = 1$

Bead	Fixed dipole	Mutual dipole	Two body	Inclusion method	Exact
1	0.318540	0.399889	0.469333	0.514543	0.507733
2	0.023898	0.059832	0.024279	0.063490	0.056234
3	0.005258	0.014335	0.005279	0.015035	0.013690
4	0.001150	0.003119	0.001153	0.003260	0.003052

The forces are computed using different models described here. Only the forces on beads 1–4 are provided since the forces on 5–8 are equal and opposite to these values.

mutual dipole method at the end, and the pairwise two-body calculation in the middle. The minimum force, $\mathscr{F}$, required to break a chain of N beads at the point between beads n and $n+1$ is given by the sum of the resultant magnetic forces

$$\mathscr{F} = \sum_{m=n+1}^{N} F_{\parallel}^{(m)}, \tag{85}$$

where $\parallel$ denotes the force component along the axis of the chain. This sum achieves its maximum value at the center of the chain, which in the case of $N = 8$ considered here is between beads number 4 and 5. It should be noted that for this specific configuration the resultant force in the middle of the chain is dominated by the dipole interactions.

The inclusion model performs exceptionally well when the particles are distributed along a line. Problems arise, however, when the configuration is no longer collinear. These configurations are present at high volume fractions [32] or when the suspension is subject to a rapidly rotating field [17]. In Fig. 12, a triangular configuration is subject to a uniform field. The forces are attractive. The results are compared with the exact force taken from [15]. In this case, the 40% error in the force at contact is reduced to 10% with the inclusion model. Although the inclusion model provides a better approximation of the force than the other models, its performance is not as good as it was in the previous cases. Extending the far-field calculation to include quadrupole moments may be a way to improve this result.

5. Summary and discussion

The purpose of this study is to develop a method to estimate accurately and efficiently the magnetic forces between paramagnetic particles that is applicable for systems of thousands of particles. An accurate quantification of the interparticle forces is necessary to determine the rheological properties of MR fluids or the performance of micro-fluidic devices, where unsteady magnetic fields or shear flows introduce viscous stresses on the self-assembled chains. Accurately describing the

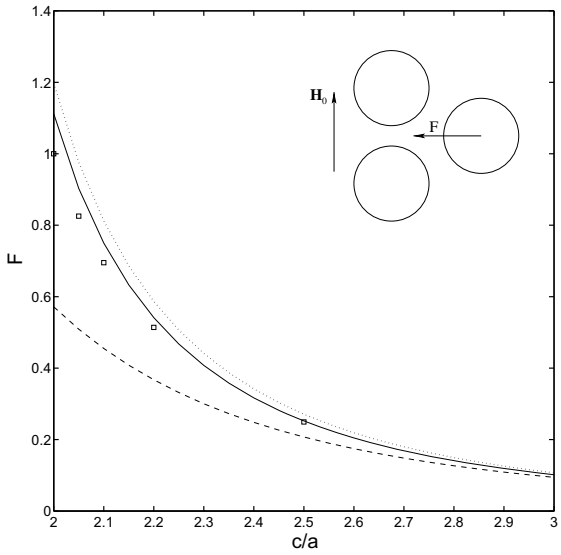

Fig. 12. Force on a bead in a triangular arrangement. The configuration is depicted in the drawing with the bead in question indicated. The data are normalized by the value of the exact solution at contact. The exact computation is provided by [15]. The inset sketch is not drawn to scale and depicts the configuration of the beads relative to the applied field and the direction of the measured resulting force. In the plot: (···) two-body calculation; (– – –) mutual dipole; (—) inclusion model; (□) exact solution.

yield strength and deformation of the structure while considering a large number of particles are necessary to determine the properties of the bulk suspension.

In the preceding sections, we have presented and described a finite-dipole model which resolves the many-body dipole interactions in MR fluids. In this model, the induced magnetization of a particle is represented as a localized Gaussian distribution of current, with characteristic length scale σ, that is then a source term in the Poisson equation for the vector potential of the magnetic field. This equation can be solved using any standard numerical solver, whether it be a finite difference or spectral code, and may also accommodate different boundary conditions on the domain. Further, the results present here can be used in the formulation of a particle-mesh Ewald method [33] if one is interested in recovering the point-dipole model. The computational work associated with the finite-dipole model comprises a fixed cost associated with solving the Poisson equation and an $O(N)$ growth associated with distributing the current sources over the grid points. A fixed numerical mesh is commonly used for simulating the fluid dynamics of a suspension of paramagnetic particles and the extra cost of solving the additional Poisson equation represents a modest increase in the overall computational effort. The choice of a/σ is discussed in the context of providing an accurate description of the force between point dipoles while ensuring the number of grid points in a particle radius is not too large.

In order to capture the near-field interactions of particles, the mutual dipole and finite dipole models have been modified to include locally higher-order multipole terms through a pairwise interaction scheme. This is based on the exact solution for two paramagnetic particles placed in a locally uniform magnetic field. This inclusion scheme is self-consistent in that it preserves both the correct far-field and near-field expansion limits, and removes the overlapping terms of the expansions. Although the inclusion scheme is intended for use with the finite-dipole model, its formulation is general and available for use in conjunction with other dipole or higher-order multipole models. The procedure yields very accurate solutions to collinear three-body problems. The scheme is not as accurate when considering other configurations but represents a significant improvement over existing methods. Further improvements may be possible by including more information from the far field (i.e. quadrupole moments). Introducing nonuniform magnetic fields into the two-body, near-field model would significantly increase the complexity of the pairwise computations.

Although only the interactions between particles of the same size and linear magnetic properties in a homogeneous suspension are considered, the methods presented here can readily be extended to more general situations. The finite-dipole method consists of representing the individual dipole moments as local distributions of current density, numerically determining the total magnetic field as a result of these sources and then using an interative process to find the induced dipole moments based on the local, volume-averaged magnetic field. By allowing a or χ_{eff} in (47) to vary between particles, the finite-dipole method can employed to address suspensions where there is dispersity in particle radius or magnetic susceptibility. Additionally, when solving for the magnetic field (see step 2 in Section 3.2), a variety of boundary conditions can be considered. For example, simulations of magnetic particles in channels may incorporate the magnetic properties of the channel walls or the magnetic field may be prescibed at the surface. One may also incorporate nonlinear constitutive models into this dipole calculation. Rather than having the dipole moments depend linearly on the volume average of the magnetic field in (47), a nonlinear function based on the material properties may be used.

The inclusion of higher order multipoles may also be adapted to more general situations. For example, where the particles in the suspension have different radii or magnetic susceptibilities, the boundary conditions of the two-body calculation can be modified to incorporate these changes. The expressions (58) and (59) will be changed accordingly with the two different values of μ and/or a now being considered. The inclusion procedure can then be carried out in the way described in the previous section. To include the higher-order effects of particle–wall interactions, one must solve Laplace's equation with the appropriate boundary conditions at the surfaces of the bead and wall. Provided the dipole moments from the far-field calculation are incorporated into the coordinate system employed in the particle/wall calculation and the far-field force between the particle and wall is known, the inclusion procedure may be used here for the particle–wall interaction. Nonlinear effects might also be included into the higher-order multipole model using a 'linearly susceptible-perfectly saturated' model. In this model, if the magnitude of the local magnetic field is below the saturation value, the material behaves linearly where as if the magnitude of the local magnetic field is above the saturation value, the multipoles will be those given by the magnetic field at saturation.

Acknowledgments

This work was supported by the National Science Foundation under grant CTS-0326702.

References

[1] D. Klingenberg, Magnetorheology: applications and challenges, AIChE J. 47 (2001) 246–249.
[2] R. Rosensweig, Ferrohydrodynamics, Dover Publications, Inc., 1997.
[3] P. Doyle, J. Bibette, A. Bancaud, J.-L. Viovy, Self-assembled magnetic matrices for DNA separation chips, Science 295 (2002) 2237.
[4] A. Rida, M. Gijs, Manipulation of self-assembled structures of magnetic beads for microfluidic mixing and assaying, Anal. Chem. 76 (2004) 6239–6246.
[5] S. Bleil, D. Marr, C. Bechinger, Field-mediated self-assembly and actuation of highly parallel microfluidic devices, Appl. Phys. Lett. 88 (2006) 263515.
[6] C. Goubault, P. Jop, M. Fermigier, J. Baudry, E. Bertrand, J. Bibette, Flexible magnetic filaments as micromechanical sensors, Phys. Rev. Lett. 91 (26) (2003) 260802.
[7] S. Biswal, A. Gast, Rotational dynamics of semiflexible paramagnetic particle chains, Phys. Rev. E 69 (2004) 041406.
[8] R. Dreyfus, J. Baudry, M.L. Roper, M. Fermigier, H. Stone, J. Bibette, Microscopic artificial swimmers, Nature 437 (2005) 862–865.
[9] E. Keaveny, M. Maxey, Spiral swimming of an artificial micro-swimmer, J. Fluid Mech. 598 (2008) 293–319.
[10] Z. Fan, R. Kumar, Biological applications of paramagnetic particles in chips, in: J. Chang, L. Kricka (Eds.), Biochip Technology, Hardwood Academic Publishers, Philadelphia, PA, 2001, pp. 291–307.
[11] L. Helseth, Self-assembly of colloidal pyramids in magnetic fields, Langmuir 21 (2005) 7276–7279.
[12] D. Klingenberg, J. Ulicny, M. Golden, Mason numbers for magnetorheology, J. Rheol. 51 (5) (2007) 883–893.
[13] J. Jackson, Classical Electrodynamics, third ed., John Wiley and Sons, Inc., 1999.
[14] J. Stratton, Electromagnetic Theory, McGraw-Hill Book Company, Inc., 1941.
[15] H. Clercx, G. Bossis, Many-body electrostatic interactions in electrorheological fluids, Phys. Rev. E 48 (4) (1993) 2721–2738.
[16] S. Melle, J. Martin, Chain model of a magnetorheological suspension in a rotating field, J. Chem. Phys. 118 (21) (2003) 9875–9881.
[17] S. Melle, O. Calderon, M. Rubio, G. Fuller, Microstructure evolution in magnetorheological suspensions governed by Mason number, Phys. Rev. E 68 (2003) 041503.
[18] E. Climent, M. Maxey, G. Karniadakis, Dynamics of self-assembled chaining in magnetorheological fluids, Langmuir 20 (2) (2004) 507–513.
[19] D. Klingenberg, F. van Swol, C. Zukoski, The small shear rate response of electrorheological suspensions. I. Simulation in the point-dipole limit, J. Chem. Phys. 94 (9) (1991) 6160–6169.
[20] H. Ly, F. Reitich, M. Jolly, H. Banks, K. Ito, Simulations of particle dynamics in magnetorheological fluids, J. Comput. Phys. 155 (1999) 160–177.
[21] L. Greengard, V. Rokhlin, A fast algorithm for particle simulations, J. Comput. Phys. 73 (1987) 325–348.
[22] D.J. Klingenberg, C.F.Z. IV, Studies on the steady-shear behavior of electrorheological suspensions, Langmuir 6 (1990) 15–24.
[23] D. Klingenberg, F. van Swol, C. Zukoski, The small shear rate response of electrorheological suspensions. II. Extension beyond the point-dipole limit, J. Chem. Phys. 94 (9) (1991) 6170–6178.
[24] R. Bonnecaze, J. Brady, A method for determining the effective conductivity of dispersions of particles, Proc. R. Soc. Lond. A 430 (1990) 285–313.
[25] R. Bonnecaze, J. Brady, The effective conductivity of random suspensions of spherical particles, Proc. R. Soc. Lond. A 432 (1991) 445–465.
[26] R. Bonnecaze, J. Brady, Dynamic simulation of an electrorheological fluid, J. Chem. Phys. 96 (3) (1992) 2183–2202.
[27] V. Namias, Application of the Dirac delta function to electric current and magnetic multipole distributions, Am. J. Phys. 47 (9) (1979) 803–806.
[28] M. Maxey, B. Patel, Localized force representation for particles sedimenting in Stokes flow, Int. J. Multiphase Flow 27 (2001) 1603–1626.
[29] S. Lomholt, M. Maxey, Force-coupling method for particulate two-phase flow: Stokes flow, J. Comput. Phys. 184 (2003) 381–405.
[30] D. Jeffrey, Conduction through a random suspension of spheres, Proc. R. Soc. Lond. A 335 (1973) 355–367.
[31] M. Allen, D. Tildesley, Computer Simulation of Liquids, Clarendon Press, 1994.
[32] J. Martin, K. Hill, C. Tigges, Magnetic-field-induced optical transmittance in colloidal suspensions, Phys. Rev. E 59 (5) (1999) 5676–5692.
[33] T. Darden, D. York, L. Pederson, Particle mesh Ewald – an N log(N) method for Ewald sums in large systems, J. Chem. Phys. 98 (12) (1993) 10089–10092.